Astron. Astrophys. 329, 1035–1044 (1998)

ASTRONOMY
AND
ASTROPHYSICS

# Silicon carbide and the 11.3-$\mu$m feature

**Renaud Papoular**[1], **Michel Cauchetier**[1], **Sylvie Begin**[2], **and Gerard LeCaer**[2]

[1] CEA/SPAM, CE Saclay, F-91191 Gif-sur-Yvette Cedex, France
[2] Laboratoire Sc. Genie, Materiaux Metalliques, Ecole des Mines, F-54042 Nancy Cedex, France

Received 11 April 1997 / Accepted 21 July 1997

**Abstract.** We have synthesized crystalline SiC powders and obtained their IR extinction spectra when embedded in KBr and CsI matrices. These spectra are not compatible with purely spherical grains. By contrast, they quantitatively support the assumptions that 1) the bulk optical constants of the grains are identical with those of thin films, and very nearly independent of crystal polytype, as measured by Spitzer et al. (1959) and 2) the granulometry is a continuous distribution of ellipsoids. All of this also applies to previously published laboratory SiC spectra.

Within this framework, we can predict the spectra of the same powders if freely suspended in vacuum. Finally, using linear combination of these, it is possible to closely fit the various spectral shapes exhibited by the IRAS/LRS data for C-rich stars.

**Key words:** methods: laboratory – stars: carbon – stars: circumstellar matter – infrared: stars

## 1. Introduction

Silicon carbide (SiC) is universally considered as the carrier of the emission band which is seen around 11.3 $\mu$m towards the circumstellar shells (CS) of many C-rich stars. This assignment may seem strange in view of the fact that 1) the measured vibrational spectrum of bulk crystalline SiC can be described by a single Lorentzian oscillator tuned at 12.6 $\mu$m (Spitzer et al. (1959), and 2) most published laboratory data on SiC powders (e.g. Friedman et al., 1981; Borghesi et al. 1985; Orofino et al. 1991) exhibit an absorption peak at a wavelength distinctly longer than 11.3 $\mu$m and different for different samples.

Moreover, the analysis, by Baron et al.(1987), of the survey data provided by the Low Resolution Spectrometers (LRS) of the IRAS satellite (IRAS Science Team, 1986) showed that, of the 535 features assigned to the SiC class (class 4n) of the LRS Catalog, only about 5% peaked at 11.3 $\mu$m. Those are the features with the highest contrast (ratio of feature peak to underlying continuum). With decreasing contrast, another peak progressively grows around 11.7 $\mu$m, which ultimately dominates the feature, leaving only a shoulder near 11.3 $\mu$m. Nearly 40% of the features peak at 11.75 $\mu$m. A hint to such a dichotomy of peak wavelengths is already apparent in the dozen features previously observed by Cohen (1984) from the ground.

As early as 1974, Treffers and Cohen invoked calculations by Gilra and Code (1971) based on Mie's theory, to explain a wide feature observed in IRC 10216, around 11 $\mu$m. Indeed, this theory predicts that the appearence of the feature is strongly dependent on the size and shape of the carrier grains. However, in spite of sparse references to the extensive work of Bohren and Huffman (1983) on shape effects, this line of attack does not seem to have been carried much further in the interpretation of laboratory or celestial SiC spectra by astrophysicists. Rather, they explain away the discrepancies by invoking the red shift due to the electromagnetic influence of the potassium bromide (KBr) matrix in which SiC powders are usually embedded for IR measurements (op. cit.; Papoular, 1988; Pegourie, 1988). Some more recent works do not even mention the problem, and take it for granted that the celestial "SiC feature" is emitted by simple small spheres of crystalline SiC, with most of the discussion bearing on the effects of structural differences (e.g. Kaito et al., 1995; Speck et al., 1996).

Lately, however, Kozasa et al. (1995) considered alternative schemes, namely core-mantle spherical grains with SiC in the core and amorphous carbon in the mantle, and vice versa. They suggest that the former is "the most plausible candidate to reproduce the 11.3 $\mu$m feature". But, although, this model reproduces the observed trend of increasing red shift of the peak with decreasing contrast of the feature, it too has its problems: in the range of observed peak positions (11.3 to 11.8 $\mu$m) the carbon mantle volume fraction is unreasonably tightly constrained ($\sim$0.5 to 0.7); the model feature is too narrow and too asymmetric as compared with observations; for small bare SiC spheres (which cannot be excluded) the feature peaks at 10.75 $\mu$m and is about 0.1 $\mu$m wide at half-maximum, at complete variance with observations. Therefore, while it is quite plausible, on thermodynamic grounds, as shown by the authors, that carbon condenses on pre-existing SiC grains, it seems necessary to pursue the search for a better model.

The difficulty lies in disentangling the combination of several effects due to size, shape and physical state (amorphous

*Send offprint requests to*: R.Papoular

or crystalline) of SiC grains, as well as embedding matrix. Understanding laboratory measurements and using them to model celestial spectra requires at least an estimation of the individual effects. With this purpose in mind, in the present work, we study SiC particles produced by two relatively new techniques: laser pyrolysis and mechanical synthesis (briefly described in Sect. 3). The particles are small enough to minimize scattering effects, which plague many previous measurements.

Instead of trying to infer the optical properties of bulk SiC from these (or other) measurements, we consistently use those given by Spitzer et al. (1959) who showed that, for all practical purposes, they apply to both $\alpha$- and $\beta$-SiC, and to both principal polarizations as well. Fortunately, the fact that these properties are quite accurately described by a single electron oscillator makes it easy to deduce the optical cross-section of any given ellipsoidal grain embedded in a given dielectric matrix. We show that the matrix does not shift the resonance feature as a whole but, rather, slants the profile. The necessary formulae are assembled in Sect. 2. Inversion of these formulae allows us to infer unambiguously a distribution of depolarization factors, $L$, for any given extinction spectrum(Sect. 3). It is then possible to compute the expected spectrum from the same particles, but in vacuum. This is done in Sect. 4 for our two powders, embedded in KBr or CsI (Cesium Iodide). Finally, it is shown that the LRS spectra of the SiC feature can be fitted with a linear combination of the two spectra expected from our powders in vacuum.

## 2. Optical behaviour of powders

For our approach to be understood and the experimental spectra to be interpreted, it is necessary to recall here some results of Mie's theory, as applied to ellipsoids of a homogeneous dielectric material. This is made much easier by the availability of the extensive work of Bohren and Huffman (1983), who, in their Chap.12, used precisely SiC as a textbook example, because its lattice vibrations are so accurately described by the single-oscillator model. SiC is an ionic crystal whose dielectric function may be written

$$\varepsilon(\omega) = \varepsilon_{0e} + \frac{\omega_p^2}{\omega_t^2 - \omega^2 - i\gamma\omega} \tag{1}$$

where $\varepsilon_{0e}$ is the constant, high frequency limit of the electronic dielectric function; $\omega_p^2 = Ne^2/m\varepsilon_0$ (MKSA units), N: valence electron density; $\omega_t$: frequency of the transverse optical mode of resonant vibration of the crystal atoms and $\gamma$: damping constant of this vibration. Due to damping, the line width of this resonance is $\gamma$ (FWHM). The low-frequency limit of $\varepsilon$ is $\varepsilon_{0v} = \varepsilon_{0e} + (\omega_p/\omega_t)^2$.

If $\varepsilon$ is written as $\varepsilon' + i\varepsilon''$, its real and imaginary parts are linked to those of the refractive index, $m = n + ik$, by

$$\varepsilon' = n^2 - k^2, \varepsilon'' = 2nk. \tag{2}$$

For the bulk material, an absorption coefficient $\alpha(\omega)$ can be defined as $4\pi k/\lambda$, which, in this case, exhibits a single peak at $\omega = \omega_t$, with a peak value

$$\alpha_t = \frac{\pi}{\lambda_t}\sqrt{\frac{\omega_p^2}{\gamma\omega_t}}, \tag{3}$$

where $\lambda_t = 2\pi c/\omega_t$ and $c$ is the velocity of light in vacuum. The absorption spectrum of grains of the same material, and size $a$, is quite different in intensity as well as frequency. Bohren and Huffman(1983) studied the case of small ($2\pi a/\lambda \ll 1$) ellipsoidal grains in detail. In this case, the self depolarization of the particle in an electromagnetic field has to be taken into account, and is of course different in the three principal orientations. Three geometrical factors are therefore defined, $L_i (i = 1, 2, 3)$,with $0 \leq L_i \leq 1$, each of which enters the corresponding expression for the absorption cross-section of the ellipsoid (against an e.m. wave whose electric field is parallel to direction $i$):

$$C_{ext}(\omega) = \pi a^2 Q_{ext}(\omega)$$

$$= \frac{v\gamma\omega_p^2}{c\sqrt{\varepsilon_m}} f(\xi, L) \frac{\omega^2}{(\omega^2 - \omega_s^2)^2 + \gamma^2\omega^2}, \tag{4}$$

where $v$: volume of particle, $\varepsilon_m$: dielectric function of the embedding matrix, $\xi = \varepsilon_{0e}/\varepsilon_m$,

$$f(\xi, L) = [1 + L(\xi - 1)]^{-2} \tag{5}$$

and

$$\omega_s^2 = \omega_t^2 + \frac{L\omega_p^2}{\varepsilon_m + L(\varepsilon_{0e} - \varepsilon_m)} \tag{6}$$

For pure crystals, $\gamma$ is normally very small, so that Eq. 4 represents a very narrow feature.

The resonant, or Frohlich, frequency, $\omega_s$, is distinctly different from the bulk frequency, $\omega_t$, and the corresponding extinction cross-section is

$$C_{ext,s} = \frac{v\omega_p^2}{\gamma c\sqrt{\varepsilon_m}} f(\xi, L), \tag{7}$$

in the principal orientation considered. The global extinction spectrum, therefore, exhibits three peaks of width $\gamma$ each. Outside the interval $[\omega_t, \omega_l]$, there is no resonance and the continuum is made up of the wings of the three resonances.

The three geometrical factors all equal 1/3 for spheres, 0, 1/2, 1/2 for needles and 0, 0, 1 for discs. The sum of the three is always unity. The larger factors correspond to the smaller principal dimensions and vice versa.

A good approximate expression for $\omega_s$ is

$$\omega_s = \omega_t \left[\frac{\varepsilon_m + L(\varepsilon_{0v} - \varepsilon_m)}{\varepsilon_m + L(\varepsilon_{0e} - \varepsilon_m)}\right]^{1/2}, \tag{8}$$

At this frequency,

$$\varepsilon'(\omega_s) \cong \varepsilon_m(1 - 1/L). \tag{9}$$

This is applicable as long as $\varepsilon_s'' \ll \varepsilon_s'$, which is not the case for a needle or a disc parallel to the electric field (when $L$=0).

From (6), $\omega_s$ is constrained to fall between the transverse ($\omega_t$) and longitudinal ($\omega_l$) optical modes of the lattice ions, corresponding to $L = 0$ and 1 respectively. Here,

$$\omega_l = \omega_t(\varepsilon_{0v}/\varepsilon_{0e})^{1/2} \geq \omega_t. \tag{10}$$

From (7) and (5), the extinction cross-section for a given particle volume, v, decreases quickly with increasing $L$ and $\omega_s$, but less so in a dielectric matrix. This is understandable since a larger $L$ corresponds to a shorter transverse size of the particle, while a stronger dielectric produces a stronger electric field.

In the degenerate case of the sphere, the three absorption peaks merge at

$$\omega_s = \omega_t \left( \frac{\varepsilon_{0v} - \varepsilon_{0e}}{1 + 2\varepsilon_m} \right)^{1/2},$$

with $\varepsilon'(\omega_s) \cong -2\varepsilon_m$. There is no linear relation between $Q_{ext}/a = \frac{4}{3}\frac{C}{v}$ and $\alpha$ of the bulk. For a sphere embedded in a dielectric matrix (e.g. Kbr, CsI...), $\varepsilon_m > 1$, hence a red shift of the resonance with respect to vacuum. Note, however, that *$\omega_s$ is independent of the particle radius; an assembly of small spheres can only exhibit one, narrow, extinction peak at a frequency depending only on the material and the matrix. A wide extinction band, therefore, can only result from a distribution of particles of different shapes.*

For real particles, the shapes are likely to be continuously distributed. From (7) and (8), there results a continuous spectrum of extinction cross-section, $C_{ext}(\omega)$, which can be deduced by eliminating $L$. Bohren and Huffman (1983) considered in detail the case of an arbitrary, continuous distribution of joint probabilities of $L$'s for ellipsoidal shapes. In particular, for a uniform probability distribution, the extinction spectrum extends nearly uniformly in the range $[\omega_t, \omega_l]$. *In such a case, the plateau extinction efficiency is smaller than the peak efficiency for a sphere by a factor* $\sim \frac{\gamma}{(\omega_l - \omega_t)}$.

So much so for for the available knowledge. What can we further infer from it for our present purposes?

First, the most important clue to the identification of an astronomical dust from its optical signature is the interval over which the latter extends, not necessarily the peak $\omega$ wavelength, which depends on the distribution of shapes.

Second, note that Eq. 7 and 8 define a one-to-one relationship between $\omega, C_{ext}(\omega)$ and $L$, for given material and matrix. It is therefore possible to infer the probability distribution of $L$'s from a measured extinction spectrum.

Third, the red shift of the peak extinction of small ellipsoids embedded in a matrix (relative to vacuum) can be deduced from (8). It depends on $L$ and, hence, on $\omega_s$: it is not the same all over the spectral extent of the signature; in particular it is nul at $\omega_l$ and $\omega_t$! *There is, therefore, no reason to "correct" IR transmission measurements of SiC in a dielectric matrix by simply blue-shifting the feature as a whole by an arbitrary amount, as has been done in the past.*

In order to quantify this in an approximate but transparent manner, we take advantage of the small relative difference between $\omega_t$ and $\omega_l$. Let $\omega$and $\omega_m$be resonant frequencies corresponding to a shape factor $L$, in vacuum and matrix, respectively. Define $x = \omega/\omega_t$, $x_m = \omega_m/\omega_t$ and $\Delta x = x_m - x$. Put $x = 1+\alpha$ and $x_l = \omega_l/\omega_t = 1 + \alpha_l$,and solve (8) for $\Delta x$, to order 2 in $\alpha$'s. Eliminating $L$, it is found that

$$\Delta x = -(\varepsilon_m - 1)\frac{\alpha(\alpha_l - \alpha)}{\alpha(1 - \varepsilon_m) + \alpha_l\varepsilon_m}. \tag{11}$$

This has a maximum of $-\frac{\alpha_l(\varepsilon_m - 1)}{2(\varepsilon_m + 1)}$ at $x = \alpha_l/2$, which corresponds to $\omega \cong (\omega_t + \omega_l)/2$.

According to (7), the peak intensity of the resonance for a given $L$ is also reduced, in a dielectric matrix, by a factor

$$r = \frac{1}{\sqrt{\varepsilon_m}} \left[ \frac{1 + L(\varepsilon_{0e} - 1)}{1 + L(\varepsilon_{0e}/\varepsilon_m - 1)} \right]^2$$

Note that this factor depends not only on the matrix but also on the particle shape.

In order for these general considerations to be applicable to the comparison between laboratory and astronomical spectra, we have yet to decide which specific constants are to be used in the formulae above. Now, SiC comes in a wide variety of crystallographic types (Schaffer, 1969) which fall roughly in two main classes:

$\alpha$-SiC: hexagonal and rhomboedric types, similar to the wurtzite variety of ZnS;

$\beta$-SiC: cubic, similar to the zincblend variety of ZnS, the more stable of the two above$\sim$1600 $^oC$ (Schaffer,1969; Tougne et al., 1993). While a cubic crystal can be expected to be described by one set of optical constants, uniaxial crystals like $\alpha$-SiC behave differently towards the ordinary and extraordinary polarizations of incident waves. However, Spitzer et al.(1959) showed that, except for a very small subsidiary resonance, there was no significant difference between the two polarisations, as far as $\alpha$-SiC is concerned. This was confirmed by Pikhtin et al.(1977).

Spitzer et al. also showed that, *near the fundamental band, and for all practical purposes, $\alpha$- and $\beta$-SiC may both be characterized by the same optical constants,* as follows:

$$\nu_t = \omega_t/2\pi c = 795 cm^{-1}, \gamma/\omega_t = 6.10^{-3}$$

$$\varepsilon_{0e} = 6.7, \varepsilon_{0v} = 10, \nu_l = 970 cm^{-1} \tag{12}$$

Thus, *there is no point in attempting to identify different celestial spectra with one of the two crystal classes,* as was done previously (e.g. Papoular, 1988).

### *2.1. Size and agglomeration effects*

While celestial grains are not expected to be larger than the Rayleigh limit, this may be the case for laboratory particles. Large sizes are indeed encountered when the grinding time is too short, or when the powder is crammed upon a solid, transparent substrate. As predicted by Mie's theory, important modifications then occur in the transmission spectrum: the feature is reduced in intensity and skewed to the red; its peak is red-shifted

and its red wing extends beyond $\nu_t$; the underlying continuum increases uniformly at first, then with an increasing slope, rising towards higher wavenumbers, due to optical scattering; This behaviour is illustrated by the measurements of Borghesi et al. (1986), on going from raw to ground (G) and, finally, ground and sedimented (GWS) powder, when the mean grain sizes decreases by 1 or 2 orders of magnitudes, and finally satisfies the Rayleigh-Gans criterion,

$$2\pi a(n-1) \ll \lambda.$$

### *2.2. Amorphicity effects*

Disorder in the crystalline structure of the material increases the damping constant, $\gamma$. This widens the Frohlich resonance and decreases its intensity in inverse proportions (Eq. 7). One may wonder if this effect could be confused with the effect of a distribution of $L$'s over a corresponding interval $\Delta L = \gamma/(\partial\omega_s/\partial L)$.

Indeed, a thin film of pure amorphous, nearly stoichiometric SiC, produced by rf sputtering (Morimoto et al., 1984) or by ion implantation (Serre et al., 1996) exhibits a Gaussian-like feature, centered at $\sim\nu_t$, about 250 cm$^{-1}$ wide at half maximum and extending from $\sim$ 400 to $\sim$ 1000 cm$^{-1}$. Contrary to shape effects, this amorphicity effect, observed in the bulk material, is highly symmetric about $\nu_t$. Both effects might coexist in amorphous grains. In that case, the feature profile can be computed from the theory above by increasing $\gamma$ accordingly. *The outcome is an extension of the feature well beyond the interval $\nu_t$, $\nu_l$ on both sides.*

To ensure that amorphicity effects are small, it is therefore necessary to test the crystallinity of the material at hand, using X-ray diffractometry, for instance.

Having considered individually, above, the various parameters which determine the position and shape of the fundamental vibrational band of a solid, we can arrange to work in the laboratory under conditions in which shape effects are dominant. This will guide us in the interpretation and comparison of laboratory and astronomical data.

## 3. Laboratory results on SiC powders

In this section, we wish to illustrate and confirm the statements of Sect. 2. For this purpose, we took advantage of the advent of two new synthesis methods used in our laboratories for more general purposes: laser pyrolysis of gaseous precursors, and mechanical synthesis by milling together pure carbon and silicon.

### *3.1. Laser pyrolysis*

Nanosized SiC powder has been synthesized by a gas phase laser driven reaction using silane and acetylene precursors and a high-power continuous wave $CO_2$ laser emitting at 10.6 $\mu$m in resonance with an infrared absorption band of silane. Detailed information on the synthesis process was given by Cauchetier et al. (1988). Sample SiC212 was obtained at atmospheric pressure under 600 W laser power, the flow rates being 600 and 300 cm$^3$/min of silane and acetylene respectively. A gray, cotton-like powder is formed. The specific surface area, as measured by adsorption-desorption of nitrogen (Brunnauer-Emmet-Teller method), is 70 m$^2$/g and corresponds to an equivalent diameter of 27nm, which agrees with transmission electron microscope photographs (Fig. 1).

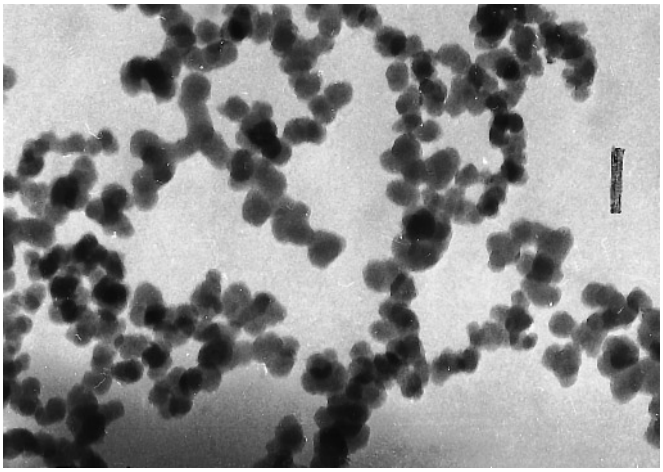

**Fig. 1.** Micrograph of an as-formed pyrolysis powder. Bar=100nm.

Chemical analysis shows the presence of 1.4 wt% of oxygen and 30.3 wt% of carbon. Neglecting hydrogen, the silicon content amounts to the remaining 68.3 wt%. From stoichiometry, the corresponding chemical composition is SiC: $SiO_2$: free carbon = 95.7: 2.7: 1.6 wt%.

$^{29}$ Si NMR spectra show the main polytype to be $\beta$ SiC with a much smaller amount of the $\alpha$ variety.

### *3.2. Mechanical alloying*

Mechanical alloying is now a widely used method to prepare all kinds of materials from elemental powder mixtures (Gilman and Benjamin,1983; LeCaer et al., 1990; Koch, 1993). A wide variety of alloys, compounds, composites have been obtained by this dry and high-energy ball-milling process often in a metastable crystalline form with a nanometric crystallite size which is typically of the order of 10 nm. Dry grinding in high-energy ball-mills is also a non-equilibrium method of processing already synthesized materials which induces changes in the ground powders such as formation of nanometre-sized crystallites with a high defect density and interface content, amorphization (Koch 1993), polymorphic transformations (for instance Begin-Colin et al. 1994), order-disorder transformations (Pochet et al. 1995). Both mechanical processes involve repeated welding, fracturing and rewelding of powder particles in a high energy ball charge. In the case of SiC, detailed studies of these processes as a function of various experimental parameters can be found in the recent literature (see for instance LeCaer et al., 1990; Matteazzi et al., 1991; Sherif El-Eskandarany et al., 1995).

Here, we have used ball-milling to refine and homogenize a commercial product of essentially the same $\beta$ polytype as in Sect. 3.1 (CERAC, Inc. (France), average initial granulometry

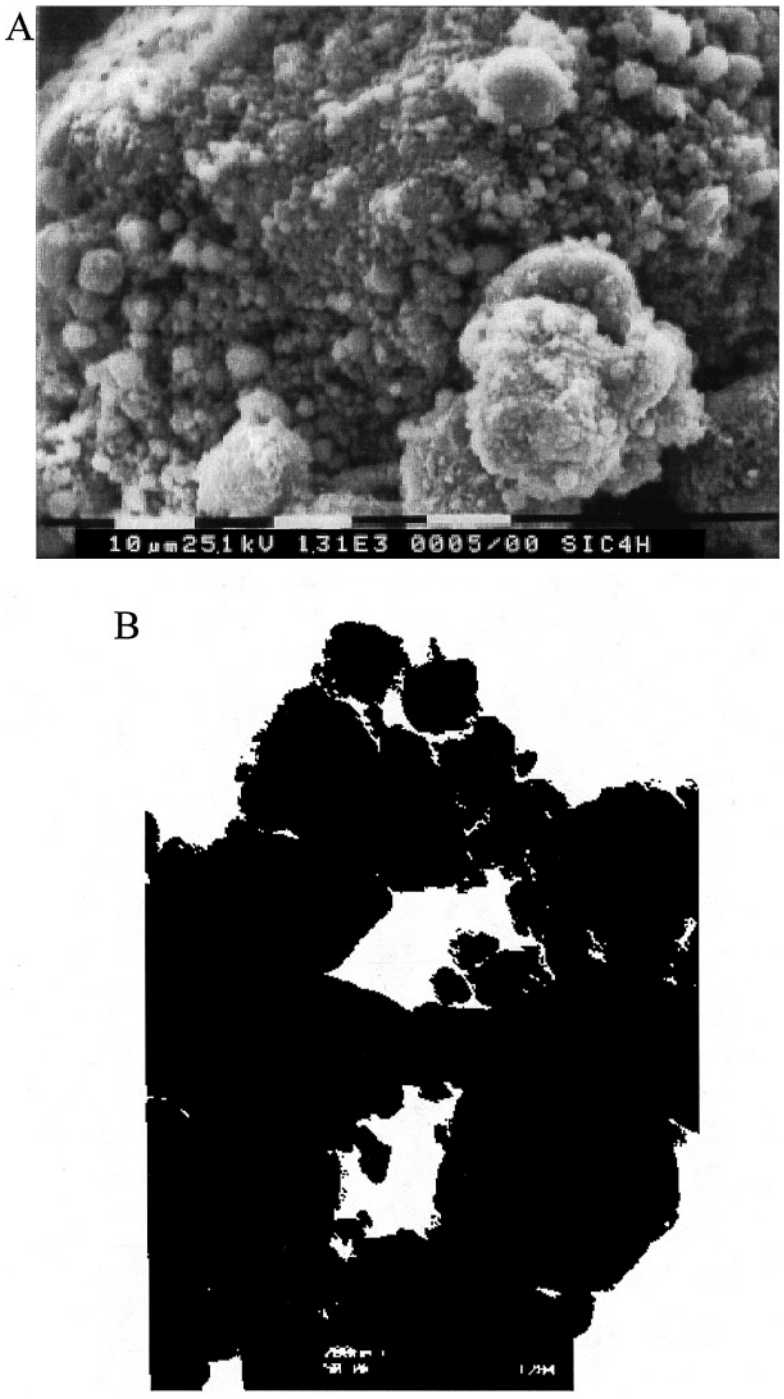


**Fig. 2a and b.** SEM **a** and TEM **b** micrographs of SiC powder ground for 4 hours.

$\sim$80 $\mu$m). The SiC powder was milled under an argon atmosphere for 4 hours in a planetary ball-mill (Fritsch Pulverisette 7) with hardened steel grinding media consisiting of a 50 cm3 vial and of seven balls of diameter close to 13 mm. The powder to ball weight ratio was 1/20. The resulting sample is designated as SiC4h.

The X-Ray diffraction (XRD) pattern of ground SiC powder is identical to the XRD pattern of the starting powder, but with broadened diffraction peaks related to crystallite sizes and strains. Grinding does not induce change in the lattice parameter of $\beta$-SiC: $a$ = 0.4361 nm and a strain $\epsilon$ of 1.2 $10^{-3}$ Å is calculated from the XRD pattern. From a morphological point of view, the ground SiC powder consists of ellipsoidal aggregates of small particles. The average size of aggregates is approximatly 100-500 nm (Fig. 2a). These aggregates are constituted of very small crystallites of about 15-20 nm as deduced from X-ray diffraction patterns and TEM observations (Fig. 2b).

### *3.3. IR Spectrometry*

Transmission spectra were obtained using KBr and CsI pellets in which small quantities of SiC powder were embedded homogeneously. A pellet is obtained by mixing about 1 mg of SiC and 300 mg of matrix powder, grinding for several minutes, and applying about 10 tons of pressure for 5 to 10 mn. The pellet is 13 mm in diameter and about 1 mm thick. It is mounted in the sample beam of a P-E interferometric spectrometer whose resolution is set at 4 $cm^{-1}$.

The absorbance spectra shown here were obtained by subtracting the spectrum of a KBr (or CsI) blank from the spectrum of an SiC-loaded pellet. Absorbances at the feature's peak range between 0.5 and 2.5. The extinction coefficient is obtained from the absorbance, $A$, by writing

$$\alpha = 2.3AS\rho/m, \tag{13}$$

where $S$=1.3 $cm^2$ is the pellet cross-section area, $\rho$=3.2 $g/cm^3$ is the density of SiC and $m$, the mass of embedded SiC (measured to 20% accuracy). Note that $\alpha$ equals $C/v$, the cross-section per unit volume *of the particles in the mixture and not of bulk SiC.* If the embedded SiC particles are *small, isolated spheres* of radius $a$, their reduced optical extinction efficiency is.

$$Q_s/a = 4\alpha/3.$$

If the particles are big by construction or by agglomeration, in the matrix, the spectrum can suffer dramatic changes: thus, Fig. 3 shows the full spectra of SiC from laser pyrolysis (sample SiC 212) embedded in KBr by careful grinding (a), and the same powder crammed over a blank KBr pellet (b). The effects predicted by theory (Sect. 2) are all observed on curve 3b. Similar effects are exhibited by embedded mechanically prepared SiC, when not ground or ground for excessively long times: 4 hours seems to be an optimum in avoiding size and agglomeration effects (hence sample SiC4h). By contrast, laser pyrolysis seems to produce consistently small particles. *Note the very weak underlying continuum absorbance across the whole spectrum.*

In the following, therefore, we consider only sample powders SiC212 and SiC4h and restrict the spectral range to the feature extent, 700 to 1000 $cm^{-1}$, as in Fig. 4 and 5.

### *3.4. Discussion*

In order to lay down sound bases for the comparison of laboratory with astronomical spectra (Sect. 4), we wish first to use our results as a test of the fundamental assumptions that: 1) the feature shape is determined mainly by the distribution of particle shapes and 2) the bulk optical constants (Eq. 12) apply to our powders.

Indeed, as expected, all extinction features are confined between ~780 and ~970 $cm^{-1}$, nearly the values of $\nu_t$and $\nu_l$. Extinction outside this range is weak, (especially for SiC212), confirming the absence of other fundamental oscillators or electronic conduction in the IR.

The red shift of the feature on going from a KBr matrix ($\varepsilon_m$ = 2.33) to the stronger dielectric CsI ($\varepsilon_m$ = 3.04), is not uniform but decreases to zero towards the edges of the feature. This test can be further quantified by using Sect. 2 to infer the *expected* feature of SiC embedded in one matrix from the *measured* feature of the same powder in the other matrix. The procedure is as follows.

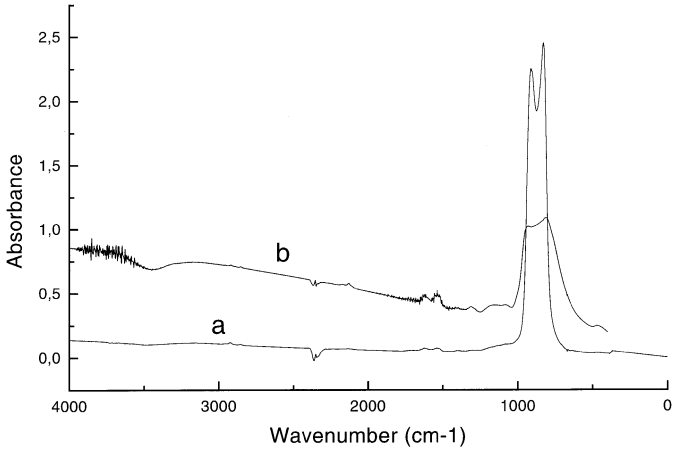


**Fig. 3.** Transmission spectra of SiC212 synthesized by laser pyrolysis: **a** homogeneously embedded in a KBr matrix; **b** crammed upon a Kbr blank pellet

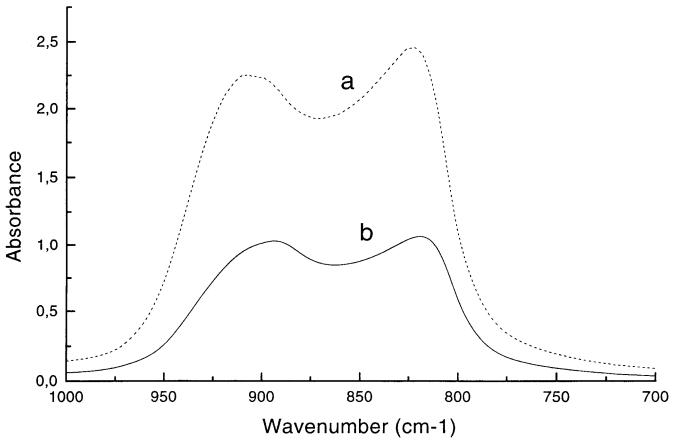


**Fig. 4a and b.** Spectral details of SiC212 powder embedded in: **a** KBr, **b** CsI.

1) Considering the weakness of the damping constant, $\gamma$, we assume that each shape parameter, $L$, contributes a single Dirac-$\delta$ resonance to the extinction spectrum, at a wavenumber $\nu$ depending on the matrix according to (8) (In this approximation, it is not possible to deal with wavenumbers outside, or near, the edges of the interval $[\nu_t, \nu_l]$, since the wings of the Frohlich resonance are artificially suppressed).

2) For each wavenumber $\nu_m$ of a spectrum taken in matrix $m$, compute $x_m = \nu_m/\nu_t$ and, inverting Eq. 8, deduce the corresponding shape parameter

$$L(x_m) = \frac{\varepsilon_m x_m^2 - \varepsilon_m}{(\varepsilon_m - \varepsilon_{0e})x_m^2 + \varepsilon_{0v} - \varepsilon_{0e}}. \tag{14}$$

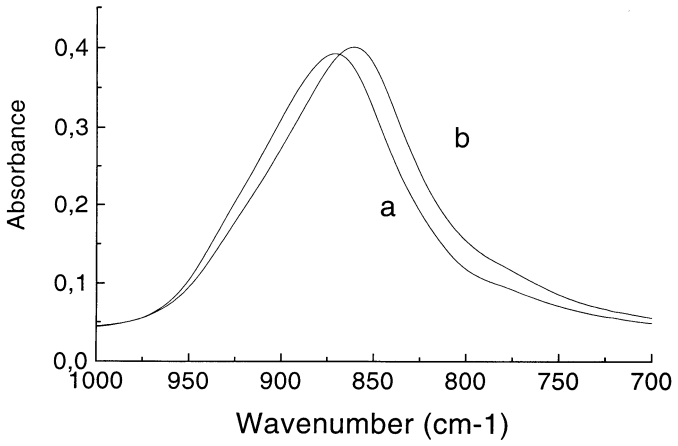


**Fig. 5a and b.** Spectral details of SiC4h powder embedded in: **a** KBr, **b** CsI.

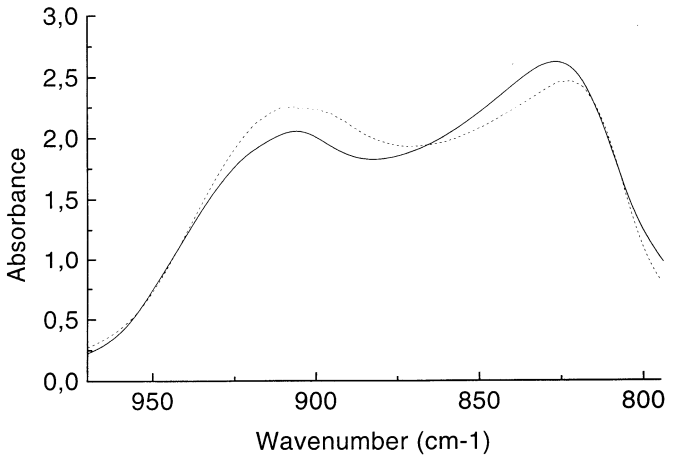


**Fig. 6.** Spectra of SiC212 in KBr. Continuous line: predicted from the measured spectrum in CsI (Fig. 2b); dashes: measured (Fig. 2a).

3) Using (8), compute the corresponding resonance wavenumber in the other matrix, $n$:

$$\nu_n = \nu_t \left[ \frac{(\varepsilon_{0v-0e})L + \varepsilon_n}{(\varepsilon_{0e} - \varepsilon_n)L + \varepsilon_n} \right]^{1/2} \tag{15}$$

where $L = L(x_m) = L(x_n)$, assuming the $L-$distribution is the same in both matrices.

4) Note that the ratio of spectral intensities, $I_n$ and $I_m$, at corresponding wavenumbers $\nu_n$ and $\nu_m$ is equal to the ratio of embedded SiC masses multiplied by the ratio of the corresponding cross-sections, $C/v$, in matrices $m$ and $n$. Hence, using (7),

$$\frac{I_n(\nu_n)}{I_m(\nu_m)} = \frac{M_n}{M_m} \sqrt{\frac{\varepsilon_m}{\varepsilon_n}} \left(\frac{1 + a_m L}{1 + a_n L}\right)^2, \tag{16}$$

where $a_m = \varepsilon_{0e}/\varepsilon_m - 1, a_n = \varepsilon_{0e}/\varepsilon_m - 1$. An intensity peak in one spectrum does not necessarily transform into an intensity peak in the other spectrum.

This procedure was applied to the spectrum (Fig. 2b) of SiC212 in CsI (matrix $m$) to deduce the expected spectrum in KBr (matrix $n$), which is compared in Fig. 6 to the measured spectrum (Fig. 4a). The fit is particularly sensitive to the exact value assumed for $\nu_t$; here, the best fit was obtained for 798 cm$^{-1}$, in agreement with Spitzer et al.'s value to instrumental accuracy. The small discrepancies in intensity are most likely ascribed to inevitable differences in particle aggregation.

Finally, compare the measured and expected extinctions. The measured values of $C_{ext}/v$ at the peak of the feature are (in cm$^{-1}$)

| | KBr | CsI |
|---|---|---|
| SiC212 | 2.3 $10^4$ | 2.9 $10^4$ |
| SiC4h | 2.8 $10^4$ | 3.6 $10^4$ |

(17)

*If* the SiC particles were all small *spheres,* we would, from Eq. 7, expect their peak extinction coefficient, $\alpha_{s,peak}$, in KBr and CsI respectively, to be 6.8 $10^5$ and 8.2 $10^5$cm$^{-1}$. Thus, the ratios of expected to measured peak extinction efficiencies are, for SiC212 and SiC4h, respectively

| | KBr | CsI |
|---|---|---|
| SiC212 | 29.6 | 28.3 |
| SiC4h | 24.3 | 22.8 |

(18)

Similar huge "discrepancies" were previously blamed on the use of bulk SiC optical constants to interpret the spectra of powders. Note, however, that micrographs show that the particles are not mostly isolated spheres. Besides, if they were, their spectrum would be a Lorentzian curve of width $\gamma/2\pi c$=4.8 cm$^{-1}$, peaking at$\sim$900 cm$^{-1}$.

Given the purity and crystallinity of our materials, *the observed spectral profiles should rather be interpreted in terms of continuous distributions of grain shapes.* In this case, it is indeed expected that the feature peak should be depressed relative to $\alpha_{s,peak}$, with the area under the peak remaining the same as in the case of spheres. In other words, the feature peak height should be inversely proportional to its width. Here, the observed widths are 137 and 102 cm$^{-1}$, for SiC212 and 4h, respectively, as compared with the Lorentzian width of 4.8 cm$^{-1}$. Hence, the expected peak extinction coefficients corrected for the shape effect

| | KBr | CsI |
|---|---|---|
| SiC212 | 2.4 $10^4$ | 2.9 $10^4$ |
| SiC4h | 3.2 $10^4$ | 3.8 $10^4$ |

(19)

in agreement with the numbers in (17), to within errors on SiC masses embedded in the pellets.

Since our fundamental assumptions are validated by this test and previous remarks, we retain these assumptions for further discussion. Thus, Fig. 7 gives, for each wavenumber, a) the calculated red shift $\Delta\nu_m$ of the feature, due to embedding in KBr, relative to vacuum, b) the depolarization factor, $L$.

We now proceed to discuss the spectra within this framework. First note that the "blue" peak of SiC212 in KBr (Fig. 4a) occurs at $\sim$905 cm$^{-1}$, close to the expected position for spheres

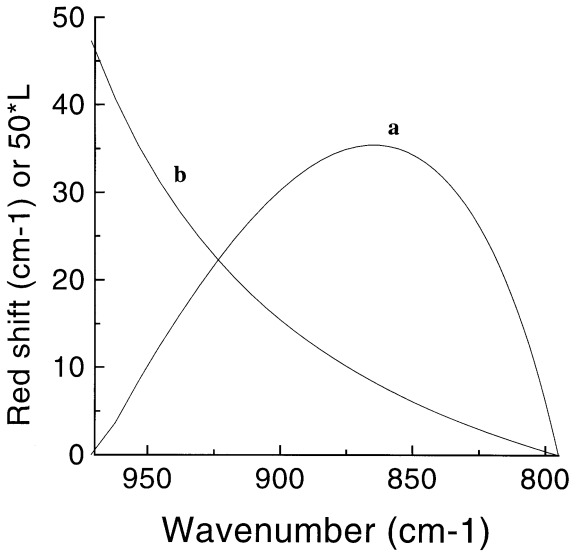


**Fig. 7a and b.** Predictions for any SiC powder in KBr. **a** Red shift $\Delta\nu$ relative to powder in vacuum; **b** depolarization parameter, $L$; both as a function of wavenumber read from the spectrum of a loaded KBr pellet.

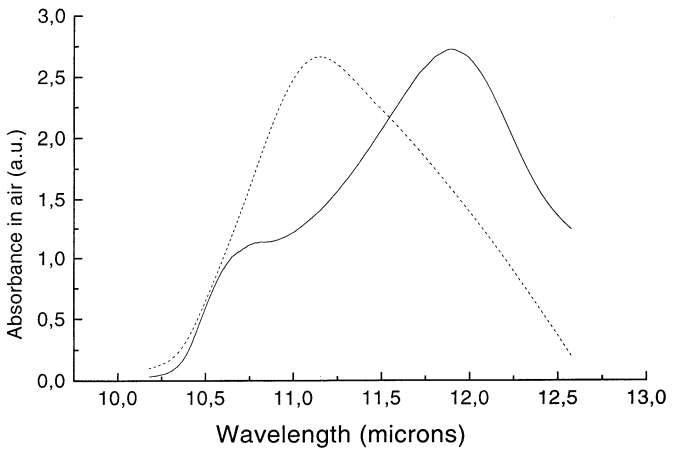


**Fig. 8a and b.** Predicted emissivity spectra of our powders in vacuum. **a** Continuous line: SiC212 (laser pyrolysis); **b** dashes: SiC4h (mechanical synthesis).

(cf. Fig. 7). This indicates a shape probability distribution favouring nearly spherical shapes, in agreement with micrographs of laser-produced powders.

The other peak in Fig. 4 (820 $cm^{-1}$or12.2$\mu$m) and the single peak of Fig. 5 (870 $cm^{-1}$ or 11.5 $\mu$m) must be due to oblate and/or prolate spheroids. The position of this peak mainly depends on the particular shape distribution, i.e. on the production process and preparation technique. Thus, the single peak in the spectra of Friedman et al. (1981) occurs near 840 $cm^{-1}$while that of 600GWS, the purest and finest powder of Borghesi et al. (1985), falls at 860 $cm^{-1}$. The samples of Koike (1987) cover the whole range from 820 to 885 $cm^{-1}$. Since all these spectra were taken in KBr matrices, it can be deduced from Fig. 5 that the corresponding $L$'s range from 0.05 to 0.25. For ellipsoids, the corresponding ellipticities fall between 0.7 and 0.88 (Bohren and Huffman, 1983), and the ratio of large to small size, between 1.4 and 50. This is compatible with the flakes and /or strings of spheroids seen under the microscope.

To us, the correlation that seems to exist between polytype and feature peak position (Kaito et al., 1994) only implies that crystal polytypes may come in prefered shapes of particles, not that they have different bulk optical constants. This is borne out by the large variety of spectra that can be obtained by the same laboratory, for the same polytype.

Only exceptionally does the literature mention a strong peak near $\nu_t$=795 $cm^{-1}$(12.6 $\mu$m). One such case is Pultz and Hertl (1966), who studied matts of fibers deposited upon a transparent substrate. The main peak occured at 795 $cm^{-1}$, corresponding to the electric field parallel to the fiber axis ($L$=0). The single, secondary peak occured at 941 $cm^{-1}$ ($L \sim 0.5$) as expected if the small dimension of the fiber is parallel to the electric field. For both peaks, the width was $\sim 40$ $cm^{-1}$, much less than $\nu_l - \nu_t$, indicating a relatively discrete distribution of shapes, as expected for this sample.

Neither small nor large spheres exhibit the 12.6 $\mu$m feature; only intermediate-sized spheres do so, but this feature is then dwarfed by the characteristic feature of spheres at $L$=1/3 (Bohren and Huffman, Fig. 12.1).

Finally, it is useful to recall here the attempt of Pégourié (1988) to infer the optical constants of $\alpha$-SiC from spectra of Borghesi et al. for this polytype, using a Kramers-Kronig analysis. The indeces he obtained were distinctly different from those of Spitzer et al. for the bulk material. This paradox can be explained away by noting that Pégourié assumed the sample particles to be spherical, although micrographs show they were not. As a consequence, the damping constant of his equivalent oscillator had to increase considerably so that the resonance could cover the whole feature width. Moreover, a near IR peak was forced into his extinction index, $k$, by the steep rise, towards short wavelengths, of the experimental spectrum he used. Such a rise is most probably due to scattering by large agglomerates, and is not visible in our spectra (Fig. 3a); neither is it compatible with Spitzer et al.'s measurements.

We conclude that all observed laboratory spectra, to our knowledge, can be interpreted by using the bulk optical properties and allowing for the distribution of particle shapes. If the latter is unknown, it can be inferred from the extinction spectrum (cf. Fig. 6), provided the particles are small enough. However, there is no way to infer the bulk optical properties from the spectrum, if the shape distribution is unknown. The assumption that the particles are spherical is generally not tenable. Even a continuous distribution is a better approximation.

## 4. Analysis of the astronomical "11.3$\mu$m" feature

The analyses of the LRS spectra presented by Baron et al. (1987) and Papoular (1988) are reconsidered here in the light of the previous discussion.

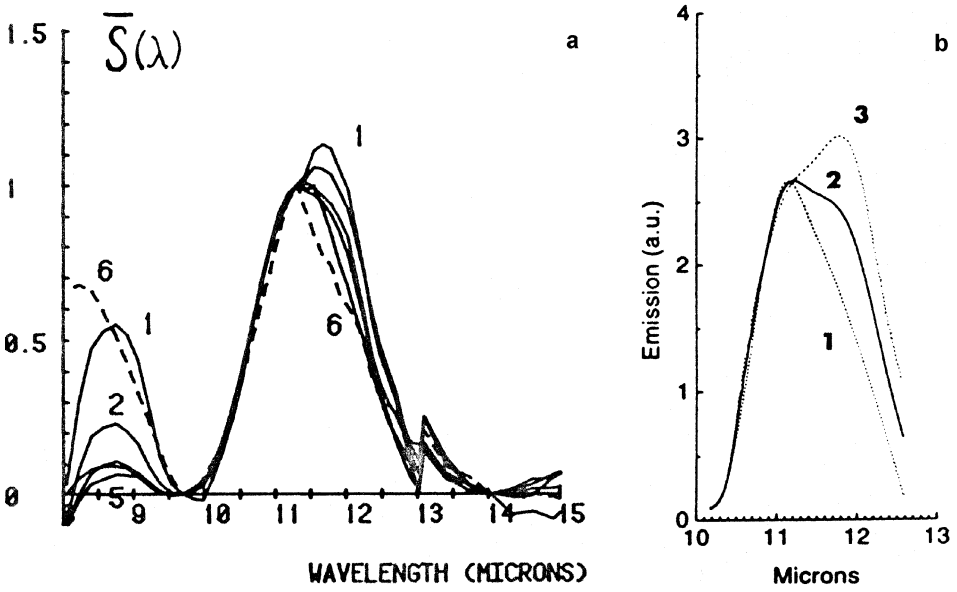


**Fig. 9. a** Shortwave spectra of SiC excess emission of the 535 C-rich stars in the LRS Catalog (Papoular, 1988); **b** linear combinations of the 2 spectra in Fig. 6: 1) $0\times$(a)+(b); 2) $0.39\times$(a)+$0.78\times$(b); 3) $0.77\times$(a)+$0.58\times$(b).

Fig. 9a represents 6 spectra, each of which is the average of from 24 to 142 spectra extracted from Class 4n of the LRS Catalog, and having closely similar profiles. In each case, a power-law continuum (passing through the spectral points at 9.7 and 14 $\mu$m) was extracted from the LRS spectrum to give the excess emission associated with the band carrier, which is shown in the figure. We are not interested, here, in the peak between 8 and 10 $\mu$m, which is probably emitted by another dust component. For the central features, however, the SiC model is relevant, since the laboratory features cover exactly the same wavelength range. However, in order to compare LRS spectra with laboratory spectra taken in solid matrices, we have first to convert the latter to vacuum. The procedure is the same as in Sect. 3.4 (Eq. 14-16), except that,here, the target matrix has $\varepsilon_n$=1. Fig. 8 shows the result for both our powders.

The feature peaks at 11.9 $\mu$m for SiC212, and 11.15 $\mu$m for SiC4h. Since the LRS spectra (Fig. 9a) exhibit peaks near 11.3 and 11.8, it is tempting to try and fit them with linear combinations of the two spectra in Fig. 8. This is done in Fig. 9b, for spectra 1,3 and 6 of Fig. 9a. *We emphasize that no arbitrary frequency shift was introduced in this procedure, and that the only free parameter in each fit was the ratio of the multiplying coefficients of the two curves in Fig. 8.* Such small discrepancies as may be seen between Fig. 9a and b are only to be expected since the grain growth and evolution processes in space are not necessarily exactly the same as in the laboratory. A more rigorous procedure would require the multiplication of the emissivities by a Planck function corresponding to the "average" dust temperature for each set of spectra. However, we checked that this has not much of an impact on the profiles or on the peak wavelengths, for temperatures between 200 and 1250K, characteristic of circumstellar dust.

As they are, these fits indicate that the diversity of the observed feature profiles can be understood in terms of different physical conditions in the dust birthplace, giving rise to various grain shape distributions. *It is not possible to explain this variety by invoking polytypes.* On the other hand, one can state that the cosmic SiC is mostly crystalline.

Goebel et al. (1995), using another classification scheme, also displayed a series of spectra obtained by averaging the LRS spectra in each of their 5 classes of 11.3 $\mu$m features. The features differ in width and peak wavelength; the latter ranges between $\sim$11.3 and $\sim$11.7$\mu$m and the overall picture is quite reminescent of our Fig. 9a. The authors interpret this variation as being due to a varying mixture of SiC and a-C:H dust in the CS shells. Papoular (1988) suggested a similar interpretation, based on the apparent correlation of the 11.7 $\mu$m peak with the peak near 8.6 $\mu$m, both of which he tentatively attributed to another, carbonaceous, dust component. However, a-C:H, for instance, also carries features at 3.4, 6.2 and 7-9 $\mu$m, which are not yet known to occur in the spectra of C stars. The recently launched ISO sattelite may help confirm (or otherwise), their existence in the future. Meanwhile, the interpretation given above seems preferable.

Roche et al.(1991) and others more recently, such as Beintema et al. (1996), have detected a feature at about 12.7 $\mu$m in various hot nebulae. Baron et al.(1987) also pointed to a feature at 12.8 $\mu$m, exhibited by 79 LRS spectra of Class 1n, on the wing of a stronger feature peaking at 11.3 $\mu$m and covering the interval 10-14 $\mu$m. It should be interesting to explore the possibility that these features be linked to the 12.6-$\mu$m feature discussed at the end of Sect. 3, in connection with fiber matts. A linear string of small, connected spheres of crystalline SiC (a more plausible structure in space) should also exhibit this feature. Unfortunately, these wavelengths are at the edges of the useful pass-bands of both spectrographs on-board the IRAS satellite, so that the feature is not easily documented in the LRS. Again, the ISO satellite should give more accurate profiles and positions.

*Acknowledgements.* We are grateful to O. Guillois for useful discussions and computations

## References


Baron, Y., de Muizon, M., Papoular, R. and Pégourié, B. 1987, A&A, 186, 271

Begin-Colin, S., LeCaer, G., Mocellin, A. and Zandona, M. 1994, Phil. Mag. Lett., 69, 1

Beintema, D., van den Acker, M. et al. 1996, A&A, 315, L369

Bohren, C. and Huffman, R.1983, Absorption and Scattering of Light by Small Particles, J. Wiley, New York

Borghesi, A., Bussoletti, E., Colangeli, L. and Blasi, C. 1985, A&A, 153, 1

Cauchetier M, Croix O. and Luce M 1988, Adv. Ceramic. Mater., 3, 548

Friedman, C., Gurtler, J., Schmidt, R. and Dorschner, J. 1981, Ap&SS, 79, 405

Gilra, D. and Code, A. 1971, BAAS, 3, 379

Gilman, P. and Benjamin, J. 1983, Ann. Rev. Mater. Sci., 13, 279

Goebel, J., Cheeseman, P. and Gerbault, F. 1995, ApJ, 449, 2461

Koch, C. 1993, Nanostruct. Mater., 2, 109

Hackwell J. 1971, PhD Thesis, cited by Huffman R. 1977, Adv. Phys., 26, 129

IRAS Science Team, 1986, A&AS, 65, 607

Kaito, C. et al. 1995, Planet. Space Sc., 43, 1271

Koike, C. 1987, in Grain Formation Workshop VIII, p48-52

Kozasa, T., Dorschner, J., Henning, Th. and Stognienko, R. 1996, Preprint 47, Jena

LeCaer, G., Bauer-Grosse, E., Pianelli, A. Bouzy, E. and Matteazzi, P. 1990, J. Mater. Sc., 25, 4726

Matteazzi, P. and LeCaer, G. 1991, J. Amer. Ceram. Soc. 74, 1382

Morimoto, A., Kataoka, T., Kumeda, M. and Shimizu, T 1984, Phil. Mag. 50, 517

Orofino, V., Mennella, V., Blanco, A. et. al. 1991, A&A, 252, 315

Papoular, R. 1988, A&A, 204, 138

Pégourié, B. 1988, A&A, 194, 335

Pikhtin, A., Prokopenko, V., Rondarev, V. and Yaskov, A. 1977, Opt. Spectrosc. (USSR), 43(4), 420

Pultz, W. and Hertl, W. 1966, Spectrochim. Acta, 22, 573

Roche, P., Aitken, D. and Smith, C. 1991, MNRAS, 252, 282

Serre, C., Calvo-Barrio, L. et al. 1996, J. Appl. Phys., 79, 6907

Sherif El-Eskandarany, Sumiyama, K. and Suzuki, K., 1995, J. Mater. Res., 10, 659

Speck., A., Barlow, M. and Skinner, C. 1996, From Star Dust to Planetesimals, NASA Sympos. Santa Clara, CA, June 24

Spitzer, W., Kleinman, D. and Walsh, D. 1959, Phys. Rev., 113, 127

Tougne, P., Houmel, H., Legrand, A., Herlin, N., Luce, M. and Cauchetier, M 1993, Diam. Rel. Mater., 2, 486

Treffers R. and Cohen, M. 1974, ApJ, 188, 545


This article was processed by the author using Springer-Verlag LaTeX A&A style file *L-AA* version 3.